Available online at www.sciencedirect.com
SCIENCE DIRECT®
Journal of Nuclear Materials 323 (2003) 123–137
journal of nuclear materials
www.elsevier.com/locate/jnucmat

Mechanisms of stress relief cracking in titanium stabilised austenitic stainless steel

M. Chabaud-Reytier [a], L. Allais [a,*], C. Caes [a], P. Dubuisson [a], A. Pineau [b]

[a] *Commissariat à l'Energie Atomique, DMN SRMA LC2M, Saclay, 91191 Gif sur Yvette, France*
[b] *Ecole Nationale Supérieure des Mines de Paris, UMR CNRS 7633, BP87, 91003 Evry, France*

Received 15 April 2003; accepted 25 August 2003

Abstract

The heat affected zone (HAZ) of AISI 321 welds may exhibit a serious form of cracking during service at high temperature. This form of damage, called 'stress relief cracking', is known to be due to work hardening but also to aging due to Ti(C,N) precipitation on dislocations which modifies the mechanical behaviour of the HAZ. The present study aims to analyse the latter embrittlement mechanism in one specific heat of 321 stainless steel. To this end, different HAZs are simulated using an annealing heat-treatment, followed by various cold rolling and aging conditions. Then, we study the effects of work hardening and aging on Ti(C,N) precipitation, on the mechanical (hardness, tensile and creep) behaviour of the simulated HAZs and on their sensitivity to intergranular crack propagation through stress relaxation tests performed on pre-cracked CT type specimens tested at 600 °C. It is shown that work hardening is the main parameter of the involved mechanism but that aging does not promote crack initiation although it leads to titanium carbide precipitation. Therefore, the role of Ti(C,N) precipitation on stress relief cracking mechanisms is discussed. An attempt is made to show that solute drag effects are mainly responsible for this form of intergranular damage, rather than Ti(C,N) precipitation.
© 2003 Elsevier B.V. All rights reserved.

1. Introduction

Stabilised austenitic stainless steels have been widely used for their mechanical properties and for their intergranular corrosion resistance. However AISI 347 (Nb-stabilised) and AISI 321 (Ti-stabilised) steels are also well known to exhibit a serious form of intercrystalline cracking in the heat affected zone (HAZ) of welded structures during service at high temperature.

This type of damage, called reheat or stress relief cracking, has received significant attention since the 1950s [1–6]. Many studies have linked this phenomenon to thermal aging, and more specifically to titanium carbide precipitation (in AISI 321 steel) which modifies the HAZ behaviour [7]. Fig. 1 presents a typical in-service intergranular crack induced in the HAZ of a component by this mechanism. The involved mechanism of intergranular cracking observed in stabilized stainless steels is schematically described as follows [4,8]. During welding, titanium carbides, possibly present in the material, are put into solution in the HAZ, near the fusion line. The welding process induces mechanical strains in grains located in this area and residual stresses. The mechanical strains produce a work-hardened microstructure, as shown in Fig. 1. Then, during service at high temperature, these residual stresses are relaxed, inducing plastic strains at the weld toes. Moreover, intragranular Ti(C,N) carbides precipitate on dislocations and contribute to the strengthening of the grains [3,8,9]. For many authors, these metallurgical modifications taking place within the HAZ are responsible for intergranular cracking during stress relaxation.

In order to improve design and to prevent this kind of intergranular cracking in structures operating at elevated temperature, a study [10] has been carried out at

* Corresponding author.

0022-3115/$ - see front matter © 2003 Elsevier B.V. All rights reserved.
doi:10.1016/j.jnucmat.2003.08.034

Nomenclature

a	crack length
W	width of CT specimen
B_{net}	net thickness of CT specimen
δ	opening displacement
P	load
σ_{ref}, L_{ref}	reference stress and length, respectively
ε	creep strain
C_1, C_2, n_1	creep law coefficients
$Rp_{0.2}$	yield stress
λ	mean distance between particles
ϕ	mean particle diameter
f	particle volume fraction
σ_{Orowan}	Orowan stress
μ	shear modulus
b	Burgers vector

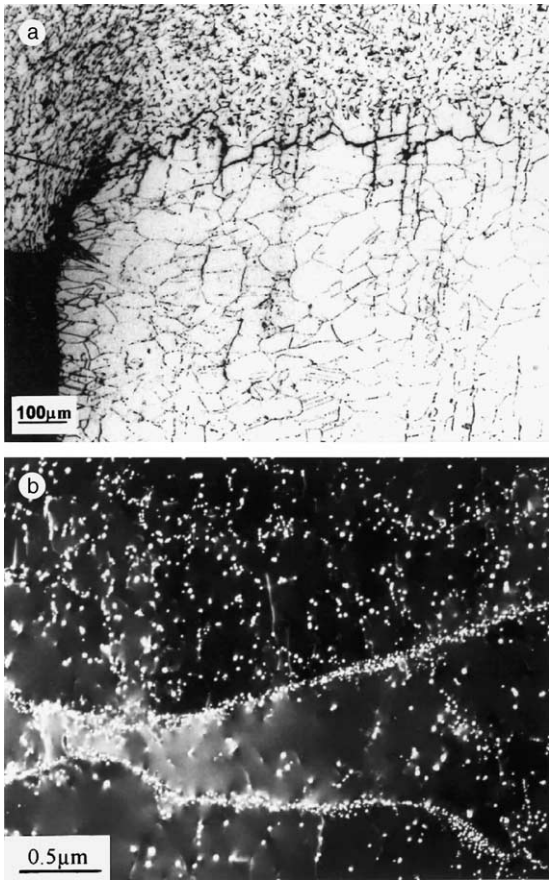

Fig. 1. In-service intergranular crack in the HAZ of an AISI 321 stainless steel weld joint: (a) optical micrograph showing the presence of an intergranular crack located near the fusion line. (b) TEM observations in dark field showing secondary Ti(C,N) precipitation.

CEA (French Atomic Energy Commission). This paper presents the results obtained in the frame-work of this large research program devoted to a better knowledge of the involved mechanisms and, in particular, to determine more accurately the role of titanium carbide precipitation. Other papers dealing with the life time assessment of real components subjected to this embrittlement mechanism have been published elsewhere [11,12].

Because of the microstructure gradient in a welded joint, the study of a real HAZ is very difficult. Therefore, in order to characterise the microstructure and the behaviour of homogeneous specimens, HAZs were simulated by an annealing heat-treatment applied to the base material which was subsequently cold rolled and aged under different conditions. Then, the effects of work hardening and aging on titanium carbide precipitation were studied using TEM observations. Moreover, the mechanical behaviour of different simulated HAZs was investigated using hardness measurements and tensile and creep tests performed on smooth bars. Stress relaxation tests on 'compact tension' (CT) specimens were also carried out to reproduce intergranular damage and to investigate the cracking sensitivity of the simulated HAZs. Finally, the role of titanium carbides on the mechanical behaviour of the simulated HAZs and on their cracking sensitivity under stress relaxation is discussed.

2. Material and experimental procedure

The material of this study is an AISI 321 stainless steel which has already been subjected to aging in service at 550 °C for 90 000 h. The material was provided as a 14 mm-thick plate. The chemical composition of this heat is shown in Table 1. It is an austenitic stainless steel, in which titanium has been added to trap carbon as Ti(C,N) precipitates and to protect the material from intergranular sensitisation.

To study the mechanical behaviour of 321 welded joints using specimens with an homogeneous microstructure, HAZs were simulated by thermo-mechanical treatments. The base plate was first subjected to a solution heat treatment at 1200 °C for 15 min. This heat-treatment has been chosen because it showed the best

Table 1
Chemical analysis of the investigated AISI 321 sheet (wt%)

C	Mn	Si	Cr	Ni	Mo	S	P	Ti	Nb	B	N
0.059	1.67	0.51	17.9	10.1	0.24	0.013	0.027	0.59	<0.05	0.0018	0.009

compromise between the amount of titanium put into solution and the growth of the grain size. A selective anodic dissolution procedure ($U = 50$ V, $I = 20$ A, in a methanol (10%) and chlorhydric acid (10%) solution) was used in order to estimate this amount of titanium. As a result of thermal treatment at 1200 °C, about two thirds of the titanium were put into solution and a 150 μm grain size was obtained (Fig. 2). This size is similar to that found in a real HAZ [8]. Then, the materials were cold rolled between 5% and 40%. Finally, they were aged between 550 and 700 °C for times between 24 and 10 000 h.

The microstructure of the different simulated materials was studied by TEM. After mechanical thinning down to 100 μm, thin foils 3 mm in diameter were prepared by electropolishing in a twin jet device. TEM observations were performed using a Philips EM 430 microscope operating at 300 kV. Microstructural evolutions due to work hardening and aging were investigated by usual techniques of electron microdiffraction and bright and dark field imaging.

The simulated HAZs were mechanically tested at 600 °C. Tensile and creep tests were carried out in air on cylindrical smooth bars with a gauge length of 20 mm and a diameter of 4 mm. The value and the gradient of temperature were controlled through three thermocouples tied to the gage length of the specimen. The temperature gradient was checked to be less than 3 °C. Tensile tests were carried out at 5×10^{-5} s^{-1} and creep tests were performed under constant load. The elongation of these creep specimens was measured with a capacitive extensometer. The initial applied stress level was chosen in order to obtain rupture times in the range of a few tens to a few thousands hours. All these specimens were cut in the middle of the plate along the transverse direction of cold rolling.

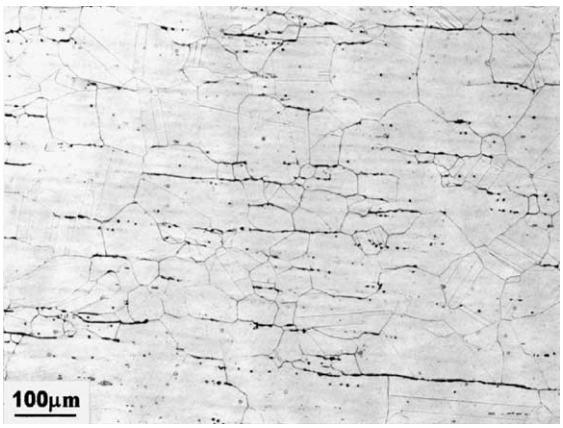

Fig. 2. Light micrograph of simulated HAZ after annealing heat treatment.

In order to study intergranular damage, uniaxial creep tests were also performed on flat specimens which were tested under vacuum. Experimental details are reported in [13]. The surface of these specimens was first mechanically polished and etched to reveal the microstructure. Then, microgrids with a mesh size of 5 μm were deposited, following a technique proposed elsewhere by [14]. Instead of sputtering a thin layer of gold, microgrids were engraved by electrochemical etching of the specimens in a perchloric acid (10%), glycerol (10%) and ethanol (80%) solution. Avoiding surface oxidation, vacuum creep tests allowed SEM observations of the specimen surface after 200 and 400 h of creep test.

Stress relaxation tests were also carried out on simulated HAZ materials. Ten millimeters thick CT specimens were cut from the plate with in-plane dimensions such as $W = 40$ mm. The load was applied along the longitudinal direction while the crack was propagating along the transverse direction. These CT type specimens were first fatigue pre-cracked at room temperature such as $a/W = 0.5$ and then side-grooved to obtain a net thickness of 8 mm. These tests were performed on a servo-mechanical machine. During these tests, crack length was measured by means of a DC potential drop (PD) technique and the load point displacement was measured thanks to a capacitive extensometer located outside of the furnace and connected to the specimen by rods fixed on the pins.

The simulated HAZ materials exhibited such different mechanical behaviours that it was impossible, for the relaxation tests, to apply the same load on each CT specimen. This is why it was decided to load them in a similar manner by taking into account their mechanical behaviour. Thus, the first step of the process consisted in determining the loading conditions of the stress relaxation tests.

For that purpose, a constant crack mouth opening rate test was initially performed on a CT specimen with the same geometry. This slow opening rate test ($\mathrm{d}\delta/\mathrm{d}t = 5 \times 10^{-6}$ mm s^{-1}) was carried out to establish a reference curve giving the load, P, as a function of the opening displacement, δ. This loading curve looks like a tensile one with a linear elastic part followed by a

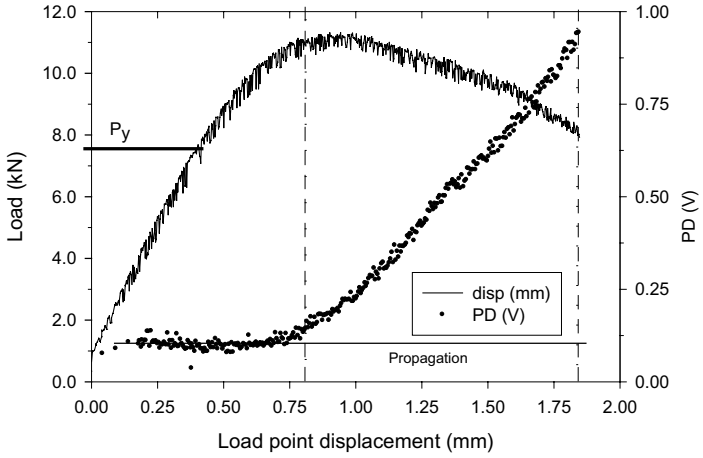

Fig. 3. Load and PD variation as a function of load point displacement during constant load displacement rate tests performed at 600 °C (D4III).

non-linear behaviour showing a maximum, as observed on Fig. 3. This curve was used to determine the apparent elastic limit load, P_y, which is defined as the onset of non-linear behaviour. For stress relaxation tests, the initial load P_0 was taken as equal to $1.2P_y$. Furthermore, the PD signal corresponding to the slow opening rate tests showed that no crack initiation occurred for the applied load level P_0 since crack initiation occurred at the maximum load, as observed in Fig. 3. As the different simulated HAZ materials show very different mechanical behaviours, retaining this procedure to determine the initial loading conditions for stress relaxation tests on CT specimens, an attempt was made to apply loading conditions with similar severities.

The loading for the relaxation tests was applied at a constant opening rate of 4×10^{-4} mm s^{-1} until the load reached the chosen level, P_0. Then the displacement corresponding to this load was kept constant during one thousand hours except otherwise stated. The specimens were finally broken in fatigue at room temperature. Crack length measurements were confirmed at the end of the tests by direct inspection. Scanning electron microscopy (SEM) was used to observe the fracture surfaces.

3. Results

3.1. TEM observations

TEM observations were made to examine the dislocation microstructure induced by cold rolling. Fig. 4(a) and (b) show the microstructure obtained with a cold rolling ratio of 5% and 10%, respectively. For 5% of thickness reduction, the microstructure consists in an homogeneous dislocation network with a low density of dislocations organized in alignments. For higher strains, cold rolling induced the formation of thin mechanical

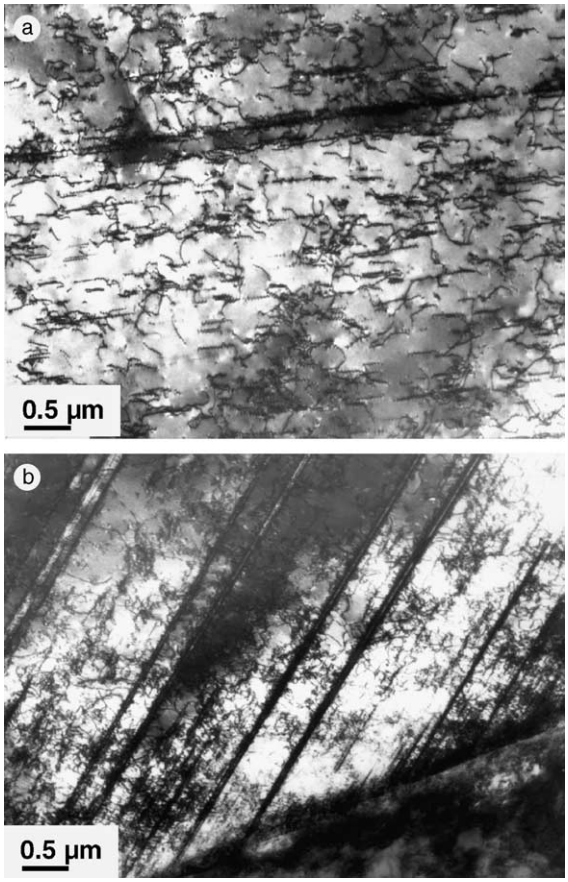

Fig. 4. TEM observations of unaged simulated HAZs of AISI 321: (a) cold rolled by 5% and (b) cold rolled by 10%.

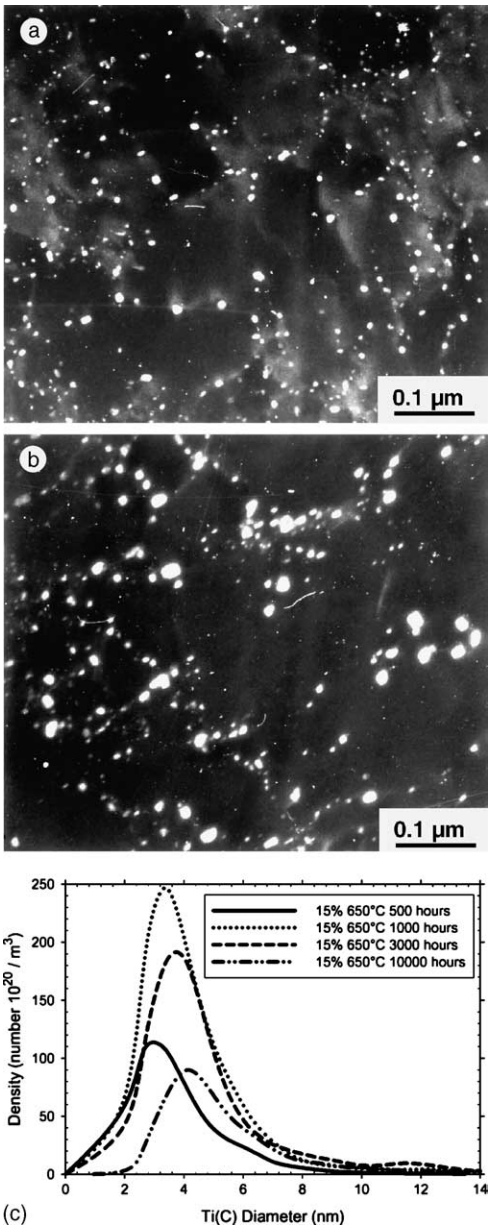

Fig. 5. Dark field TEM observations: (a) 15% cold rolled HAZ aged at 650 °C during 500 h and (b) 15% cold rolled HAZ aged at 650 °C during 10 000 h. (c) Histogram of Ti(C,N) distribution observed during aging.

twins and cells of dislocations which are characteristic of cold working in stainless steels [15].

The aging effect on the microstructure and more especially on Ti(C,N) precipitation was also investigated. The influence of aging duration was studied at 650 °C on a 15% cold rolled material. The thin twins induced by cold rolling were found to be stable all along aging. Moreover, chromium carbides and sigma phases were observed to precipitate at grain boundaries. Titanium carbide precipitation observations corresponding to aging times of 500 and 10 000 h are presented using dark field technique in Fig. 5. It can be observed that this precipitation occurs on dislocations and appears very fine. Moreover, the superposition of the particle density histograms (Fig. 5(c)) reveals a significant effect of the aging duration at 650 °C. As reported in Table 2, the mean diameter increases with the aging time as well as the volume fraction of precipitates but the number of particles decreases from 1000 h. Therefore, it seems that after the saturation of the precipitation sites, these titanium carbide particles coarsen.

The effect of aging temperature between 600 and 650 °C was also studied on a 15% cold rolled material which was aged during 10 000 h. The mechanical twins due to the cold rolling were observed to be stable during the aging at both temperatures, and the dislocation network was also observed to remain very dense. However, it was observed that grain boundary precipitates (chromium carbides and sigma phases) were smaller at 600 °C than at 650 °C, as expected.

Furthermore, the aging temperature plays a significant role for secondary titanium carbide precipitation. The comparison of TEM observations in dark field (Figs. 5(b) and 6(a)) shows that the particles precipitated at 600 °C are much smaller than those formed at 650 °C. Quantitative results are given on histograms of Fig. 6(b) and in Table 2. In particular, a higher density of particles is observed at 600 °C, compared to 650 °C. It seems, therefore, that coarsening is more difficult when the aging temperature is reduced.

The effect of the amount of cold rolling on Ti(C,N) precipitation was studied between 5% and 15% with an aging time of 3000 h applied at 650 °C. The dark field pictures can be observed on Fig. 7(a) and 7(b), while quantitative results are reported in Table 2. The more the material is cold rolled the finer and the more numerous the particles appear. Therefore it can be noticed that, by inducing a denser dislocation network, cold rolling increases the number of nucleation sites for Ti(C,N) precipitates. This leads to a finer and denser precipitation.

3.2. Mechanical properties

The effects of cold rolling and aging on the hardness of simulated HAZs are presented in Fig. 8. It can be noticed that for a moderate amount of cold rolling (up to 10%), aging at 650 °C leads to an increase of hardness. Moreover, this effect was found to be more important when the aging temperature was increased [10]. On the other hand it is observed that aging leads to a softening effect when the amount of cold rolling is higher than 15%. This effect was found to be more pronounced with an increase of the aging temperature [10]. These

Table 2
Thermo-mechanical treatment conditions and secondary Ti(C,N) precipitation characteristics for different simulated HAZs

Reference	Cold rolling (%)	Aging duration (h)	Temperature of aging (°C)	Average diameter (nm)	Diameter max. (nm)	Density (nber $10^{21}/m^3$)	Volume fraction (%)
A.3.III	15	500	650	3.8	13.1	7.7	0.036
A.4.III	15	1000	650	4.2	17.5	11.2	0.075
A.5.III	15	3000	650	4.7	21.1	9.4	0.105
A.7.III	15	10 000	650	5.5	23.23	6.9	0.135
A.7.II	15	10 000	600	3.9	11.69	8.9	0.035
C.5.III	5	3000	650	8.6	21.1	5.1	0.277
Aged base metal	0	90 000	550	16.9	55.3	0.54	0.556
Service cracked HAZ	?	90 000	550	16	38.5	1.4	0.468

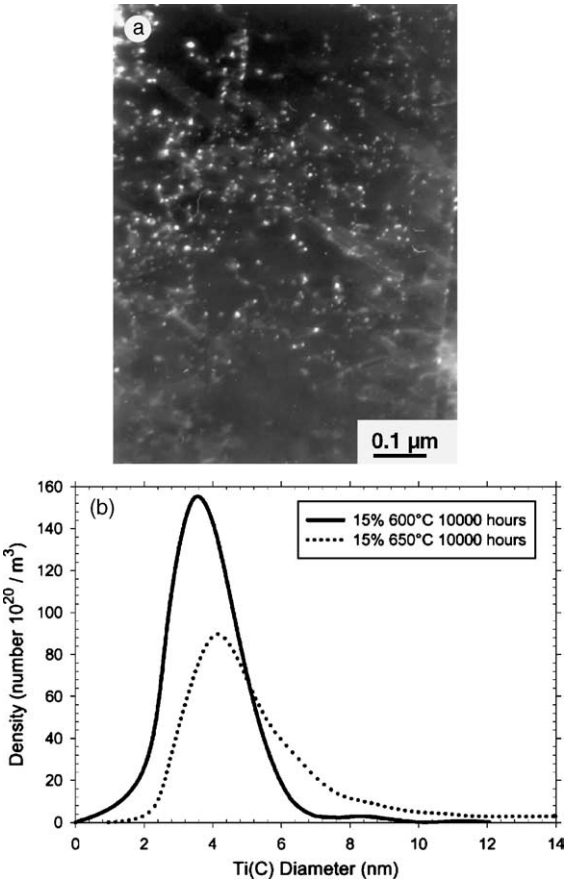

Fig. 6. (a) Dark field TEM observation of 15% cold rolled HAZ aged at 600 °C during 10 000 h. (b) Histogram of Ti(C,N) distribution after 10 000 h of aging at 600 and 650 °C.

results can be compared with TEM observations. A high cold rolling ratio induces fine and numerous titanium carbides precipitates which can slow down the dislocation motion necessary for recovery and cause a hardening effect. But this interpretation must now be completed. The mechanism described above is noticed for a moderate cold rolling ratio and our observations confirm previous studies [8] on 347 stainless steel deformed by 1%, 3% and 5%. In this work, the observed hardening was linked to the niobium carbide precipitation on the dislocations which have been introduced before aging.

For a high cold rolling ratio, aging leads to a rearrangement of the dislocation network and the hardening effect of carbide precipitation could be hidden by thermal recovery. This can explain the observed decrease of the hardness during aging.

The tensile properties of the different HAZs are presented on Fig. 9 and in Table 3. After a moderate cold rolling (0%, 5% or 10%) aging leads to an increase of the yield stress. Moreover, a reduction of the strain to failure is noticed. This phenomenon is amplified when the aging temperature is higher. On the contrary, if the material is highly pre-deformed (40%), aging leads to a decrease of the yield stress associated with a significant improvement of the ductility.

Therefore, these tensile tests performed on HAZs materials aged at 650 °C confirm that aging can be responsible for a hardening effect if the pre-deformation is moderate (up to 10% of thickness reduction), but can also be associated to a softening effect above 15% of cold rolling. Once more, aging effects could appear as a competition between precipitation hardening effect due to Ti(C,N) particles and softening effect associated to dislocation thermal recovery.

The aging effect on the creep properties of the different simulated HAZs materials (15% of cold rolling) are presented on Fig. 10. Thermal aging applied before the test systematically reduces the time to rupture and increases the minimum creep rate whereas creep ductility remains constant: creep strain at the end of secondary creep is within the range of 0.5–1.2%. This effect is observed for all the studied pre-deformations (0%, 5% and 15%). These creep results are therefore quite different

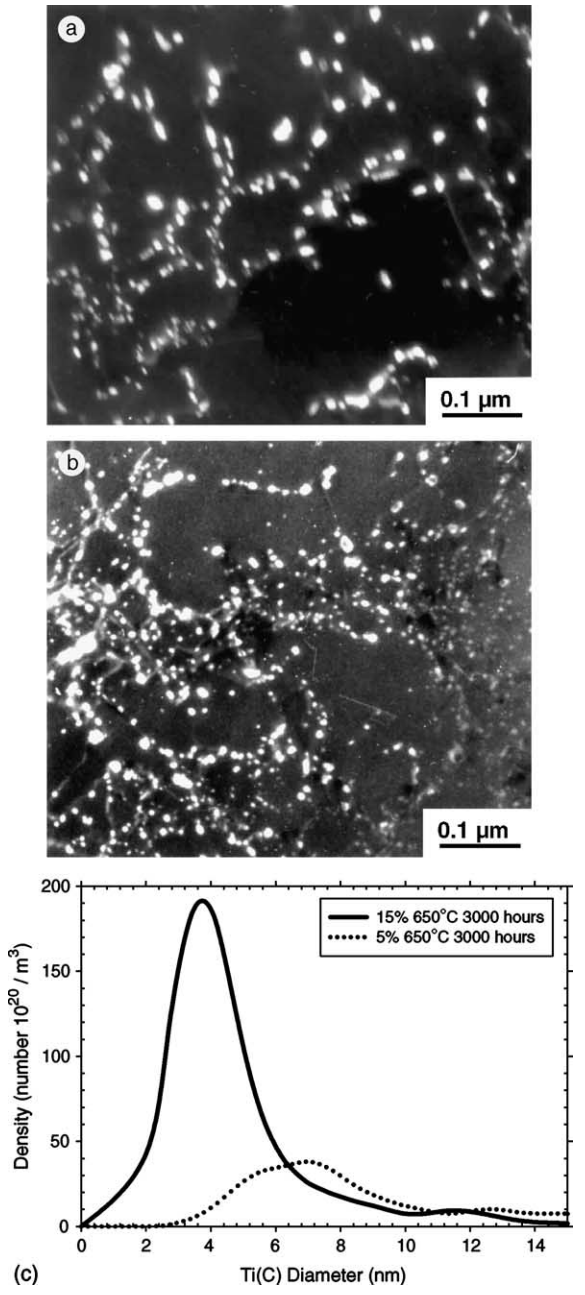

Fig. 7. Dark field TEM observations: (a) 5% cold rolled HAZ aged at 650 °C during 3000 h and (b) 15% cold rolled HAZ aged at 650 °C during 3000 h. (c) Histogram of Ti(C,N) distribution after 3000 h of aging at 650 °C for 5% and 15% cold rolled materials.

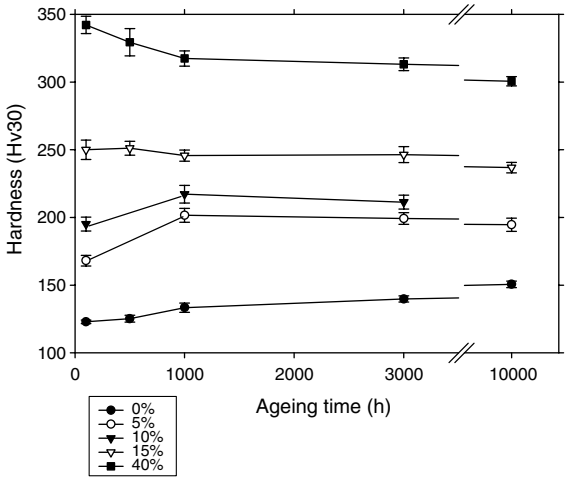

Fig. 8. Hardness as a function of aging time at 650 °C for various simulated HAZs.

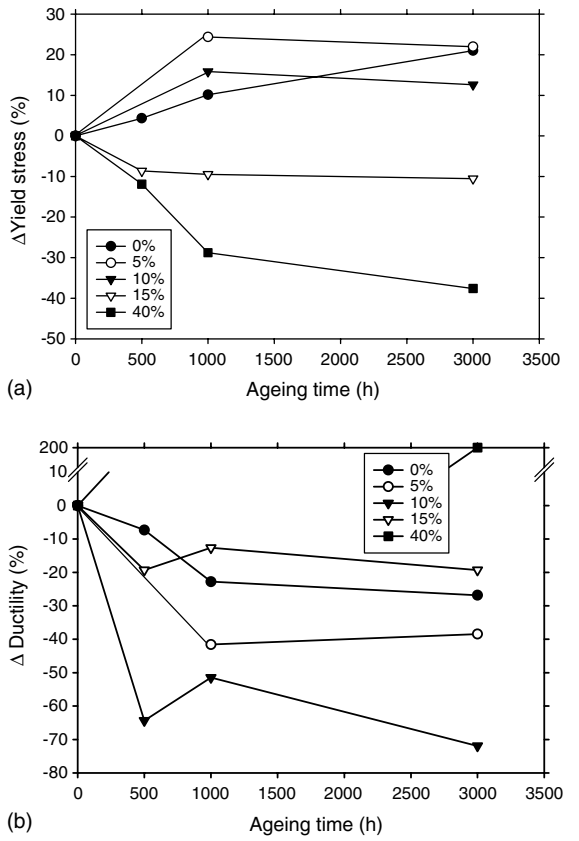

Fig. 9. Effect of aging time at 650 °C on: (a) relative variation of yield stress, (b) relative variation of strain to failure.

from those observed for tensile properties. These results confirm other ones obtained on stabilised stainless steels [16–18] but there is no general agreement about the involved mechanism. Three main questions can be raised when an attempt is made to identify these mechanisms. Is it the growth of the particles that facilitates the dislocation displacements [16]? Does the static precipitation

Table 3
Tensile properties at 600 °C of unaged simulated HAZs

Reference	Cold rolling (%)	Yield stress (MPa)	Ultimate tensile stress (MPa)	Uniform elongation (%)
O.6.I	0	138	459	24.6
C.6.I	5	246	460	19.0
D.6.I	10	309	486	17.1
A.6.I	15	475	570	5.7
B.6.I	40	681	772	1.4

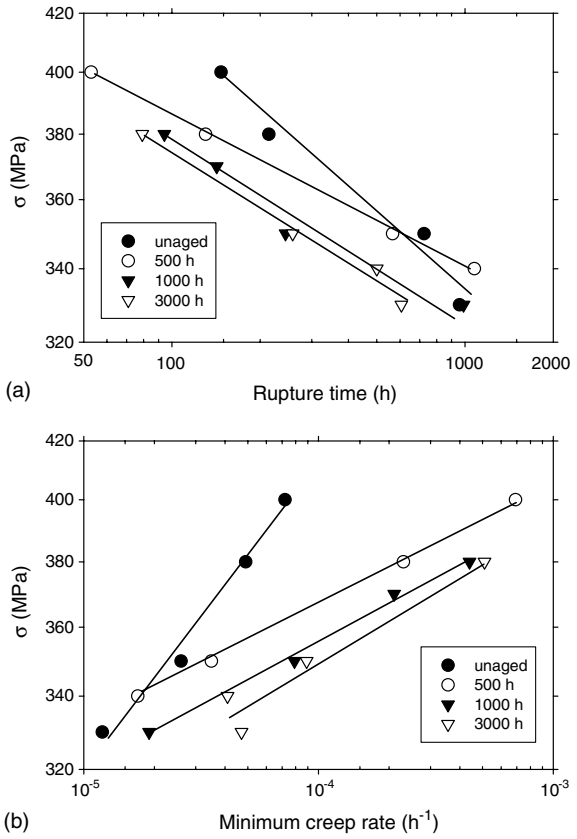

Fig. 10. Effect of aging time at 650 °C on 15% cold rolled HAZs: (a) creep rupture time at 600 °C, (b) minimum creep rate at 600 °C.

of the particles lead to innocuous carbides, reducing thereby the precipitation possibilities of other particles during the test that could be an obstacle for the dislocation motion [19]? The creep properties could also be controlled by the elements in solid solution in the austenitic matrix or by grain boundary sliding [18]. Causing the Ti(C,N) precipitation, could the aging also lead to an increase of the creep rate by a reduction of the solute drag effect?

In order to study the intergranular damage involved in the reheat cracking mechanism, a vacuum creep test

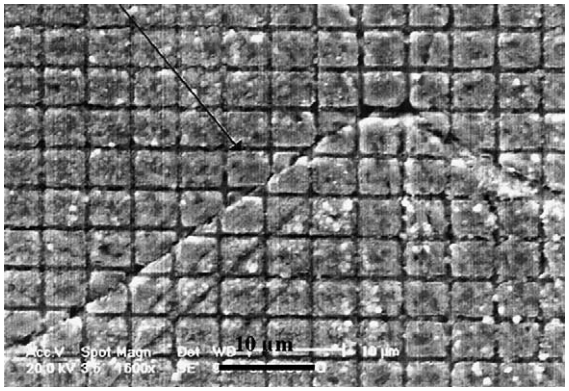

Fig. 11. SEM surface observations of simulated HAZ (15%, aged at 650 °C during 1000 h) after 200 h of creep test at 600 °C under 330 MPa.

has been performed with an applied stress of 330 MPa on a pre-deformed and subsequently aged simulated HAZ (15% cold rolled, aged at 650 °C during 3000 h). Surface observations at creep interrupted time allowed us to study grain boundary sliding and intragranular creep deformation. Fig. 11 shows that intergranular damage at grain boundary triple point and grain boundary sliding occurred for a very small value of overall creep strain (0.8%). Furthermore, the comparison between initial and strained microgrids was used to estimate the intragranular creep strain which, in that case represents 85% of the total creep deformation. Therefore the contribution of grain boundary sliding to overall creep strain is small and is not responsible for the creep rate increase observed after aging. On the over hand, grain boundary sliding might contribute to the development of intergranular damage.

3.3. Mechanical tests on CT specimens

In order to validate the HAZs simulation approach, on attempt was made to reproduce on laboratory specimens the stress relief cracking observed in components. Relaxation tests on CT specimens were chosen since the corresponding loading conditions are close to those existing in real components submitted to residual stress relaxation. Indeed, during the initial step of this me-

chanical test elastic energy is stored in the specimen as occurs in a welded component containing residual stresses. Then in these relaxation tests, the load is relaxed when the displacement is maintained constant at high temperature. These tests performed on the simulated HAZs are also useful to evidence the sensitivity to intergranular cracking as a function of the simulation parameters (cold rolling ratio, time and aging temperature).

As mentioned previously, the first step consisted in performing slow opening rate tests on CT specimens to determine the loading conditions of relaxation tests. All the experimental conditions and results are reported in Table 4 for both kinds of test on CT specimens.

The load–displacement curves obtained with low opening rate tests for the most aged simulated HAZ are consistent with the mechanical behaviour observed on smooth bars, as shown in Fig. 12. Indeed, cold rolling leads to an overall hardening effect. On the contrary, the unaged simulated HAZs curves which should present the highest value of maximum load in regard to their uniaxial mechanical behaviour are located below the curves corresponding to aged materials. This apparent inconsistency is due to the fact that, for these simulated HAZs, crack initiation occurs much earlier than in aged HAZs. Furthermore, the crack propagation lengths of the aged HAZs are lower than those measured on unaged HAZ although the crack mouth opening is higher. Consequently, this mechanical test shows that the unaged HAZ material is more sensitive to intergranular cracking than the aged material. Two representative fracture surfaces of these low opening rate tests are presented on Fig. 13. For the unaged HAZ (Fig. 13(a)), the fracture surface is entirely intergranular, with smooth grain facets. For aged HAZs (Fig. 13(b)), the fracture surface appears very different and more tortuous. Some intergranular facets can also be found as in unaged material but in this case, they are covered with dimples. The presence of these dimples can be explained

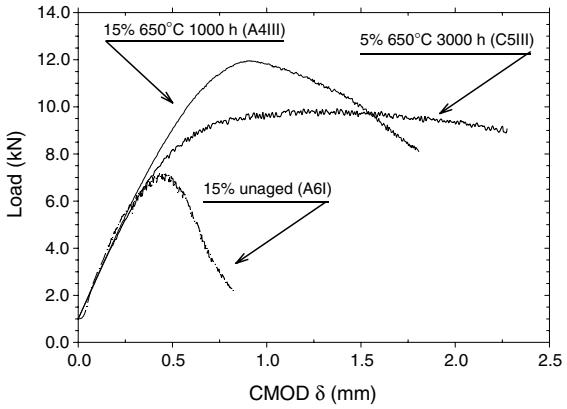

Fig. 12. Load–displacement curves during strain rate tests performed at 600 °C on various simulated HAZ.

Table 4
Loading conditions and results of slow constant crack mouth opening rate tests and relaxation tests on CT specimens

Reference	Cold rolling (%)	Aging duration (h)	Temperature of aging (°C)	Constant opening rate test			Relaxation test				
				$\Delta\delta$ (mm)	P_{max} (kN)	P_y (kN)	P_{relax} (kN)	P_{final} (kN)	δ (μm)	Test duration (h)	a (mm)
MB	0	90 000	550	3.1	7.05	4.80	5.80	2.34	366	1078	0
O5III	0	3000	650	3.23	8.43	4.20	5.10	3.14	395	1052	0
C5III	5	3000	650	2.3	9.91	6.50	7.90	5.42	466	1075	0
C4III	5	100	650	1.86	9.92	6.80	8.20	5.68	475	1071	Few grains
C6I	5	0	–	1.37	9.13	6.50	7.80	5.24	521	1024	Few grains
D5III	10	3000	650	2.2	10.74	8.40	10.10	6.59	565	1071	1.47
D4III	10	1000	650	1.29	10.63	7.40	8.90	5.95	508	1071	1.849
D6I	10	0	–	1.26	9.30	7.00	8.40	6.24	480	422	1.25
A5III	15	3000	650	1.9	11.82	8.50	10.30	6.44	582	1076	1.33
A4III	15	1000	650	1.85	11.96	8.50	10.34	6.26	531	1077	0.947
A6I	15	0	–	0.823	7.20	5.30	6.50	1.40	293	1025	1.63
A6I	15	0	–	0.824	7.30	5.30	6.50	5.80	295	32	1.11
304H	15	0	–	1.23	6.40	3.90	4.65	2.79	330	30	1.8
Hot cold rolled	15	0	–	0.795	7.19	5.20	6.25	4.29	366	379	2.7

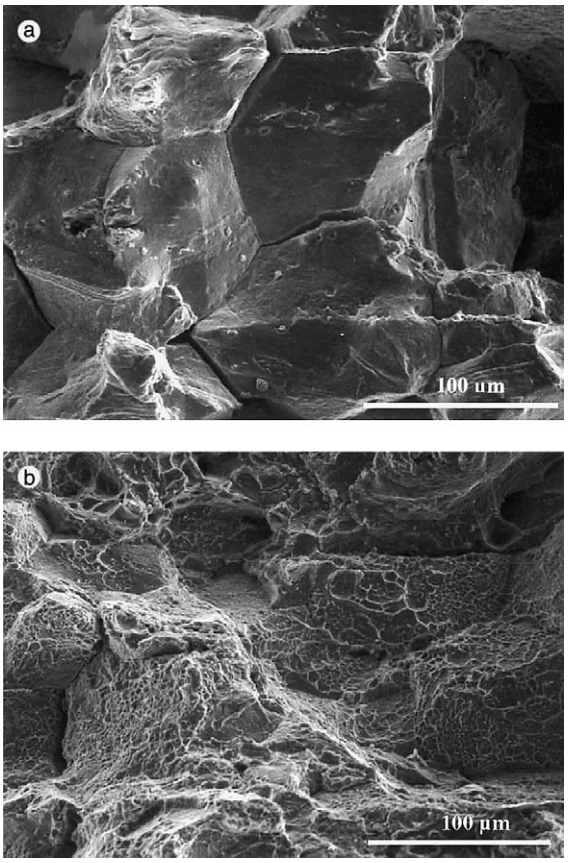

Fig. 13. Fracture surface of a CT specimen after low crack mouth opening rate test for: (a) strained (15%) and unaged simulated HAZ, (b) strained (15%) and aged simulated HAZ.

by the presence of particles located at grain boundaries. These particles are precipitated during aging.

The majority of the relaxation tests led to intergranular propagation, as indicated in Table 4. In C6I and C4III specimens, only a few number of grain decohesions were observed along the crack front. In these specimens, we considered that creep crack initiation has not taken place. Since relaxation tests on CT specimen on base metal do not lead to intergranular propagation [20], we can consider that simulated HAZ are extremely prone to intergranular cracking. It was possible to establish an intergranular cracking sensitivity diagram using these results (Fig. 14). This diagram indicates for each tested simulated HAZ the existence of intergranular propagation as a function of aging and cold rolling conditions. Fig. 14 clearly shows that the limit of intergranular cracking sensitivity is given by a critical value of cold rolling within the range of 5–10%. The aging effect seems to be of secondary importance compared to the pre-deformation effect. These results are different from those published in the literature [4,9]. They show that aging does not favour intergranular cracking since after about 1000 h of stress relaxation and for a given cold rolling ratio, a more aged HAZ leads to a lower crack propagation length (see Table 4) except for D6I specimen for which the relaxation test was interrupted after only 422 h due to an experimental problem.

For all simulated HAZ conditions leading to crack propagation during stress relaxation test, the observed fracture surfaces are intergranular. As for the constant opening rate test, two kinds of fracture surface can be distinguished: the fracture surface of cold rolled and aged materials is clearly intergranular, with many dim-

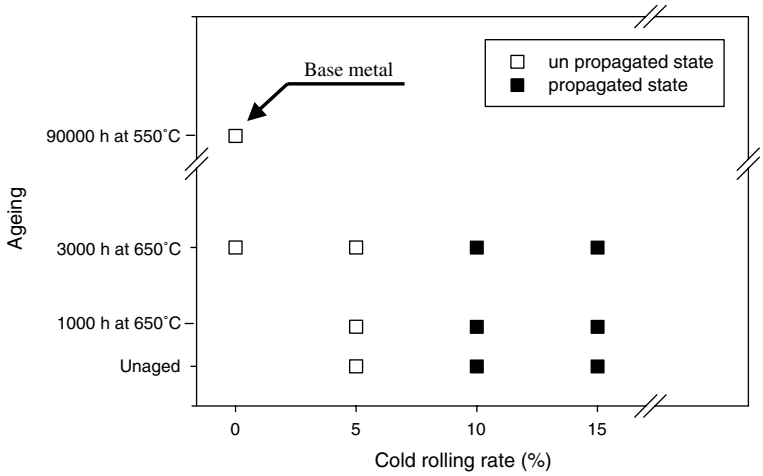

Fig. 14. Intergranular cracking sensitivity diagram indicating the presence of intergranular crack propagation in simulated HAZs during relaxation test on pre-cracked CT specimen.

ples on the grain facets (Fig. 16(b)). This reveals a creep fracture governed by the growth of cavities at grain boundaries. On the other hand, the fracture surface of the cold rolled but unaged HAZ is also intergranular but presents no dimple (Fig. 16(a)).

The effects of the rolling temperature and of the environment were also investigated. A simulated HAZ was obtained by rolling at 650 °C with a thickness reduction of 15% and subsequently tested under stress relaxation conditions. In this specimen as in the cold rolled one, intergranular propagation was observed and the length of the obtained crack was similar to that measured on the material pre-deformed at room temperature. A relaxation test was also achieved in vacuum in order to avoid any oxidation effect. This test was performed on an unaged HAZ material strained by 15%. The obtained crack length was a little bit lower than that obtained in air but the vacuum test duration was also shorter because of experimental difficulties. This test strongly suggests that the environmental effect on intergranular crack propagation observed in these conditions is quite limited.

The observation of the load relaxation curves shown on Fig. 15, indicates that the more aged is the HAZ the smoother is the curve. In particular, one can notice on the relaxation curve of the A6I HAZ (strained 15% and unaged) abrupt decreases of the load at the beginning of the test. One can wonder if these large load jumps are not due to a sudden crack propagation over a given distance. This is the reason why we have attempted to calculate the load decrease induced by a crack advance Δa. For a crack of length a, the reference stress (σ_{ref}) applied to the specimen can be calculated from the limit load analysis as [21]:

$$\sigma_{ref} = \frac{P}{m(a/W)B_{net}W}, \tag{1}$$

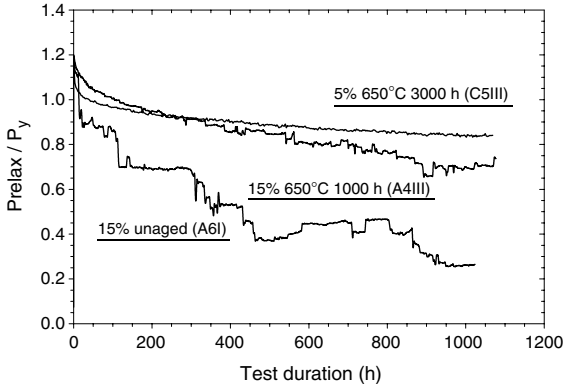

Fig. 15. Load evolution during relaxation tests on three CT specimens.

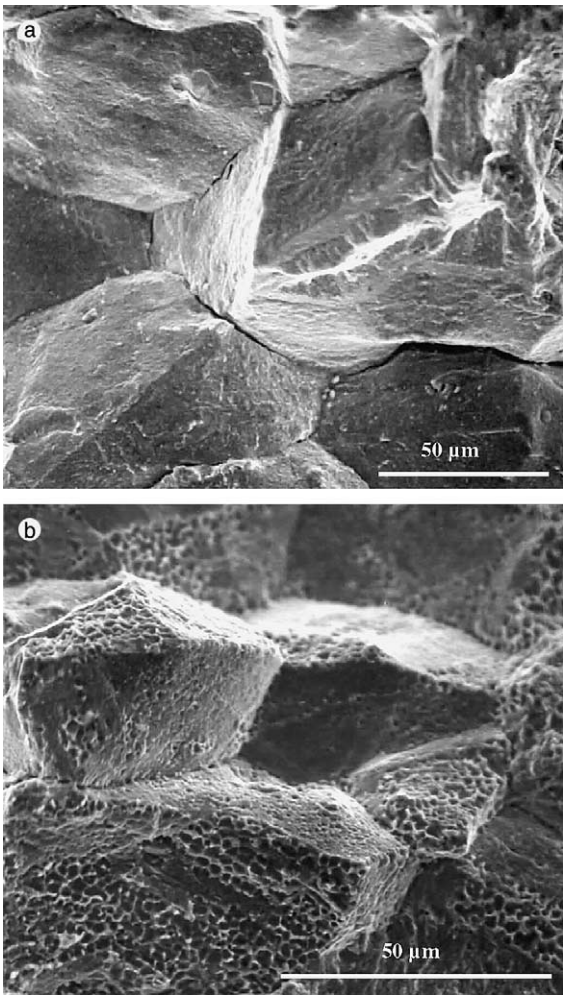

Fig. 16. Fracture surface of CT specimens after relaxation test for: (a) unaged and strained (15%) HAZ, (b) aged and strained (15%) HAZ.

where, for plane stress conditions, $m(a/W)$ is expressed as:

$$m(a/W) = \left[\left(1 + \frac{(a/W)}{q-1}\right)^2 + \frac{(1-(a/W))^2}{q-1}\right]^{1/2} \quad \text{with } q = 2. \tag{2}$$

The reference length, L_{ref}, may be determined from the uncracked ligament under plane stress conditions [21] as:

$$L_{ref} = \frac{2}{3}(W - a). \tag{3}$$

From the primary creep law, $\varepsilon = C_1 \cdot \sigma^{n_1} \cdot t^{C_2}$, a displacement law can be expressed as:

$$\delta = L_{ref} \cdot \varepsilon. \tag{4}$$

Finally one obtains:

$$\delta = \frac{2}{3} \cdot (W - a) \cdot C_1 \cdot t^{C_2} \cdot \left(\frac{P}{m(a/W) \cdot B \cdot W} \right)^{n_1}. \quad (5)$$

The crack advance, Δa, due to the load decrease ΔP can easily be calculated with Eq. (5) since, during the relaxation test, the opening displacement is maintained constant. It is given by:

$$(W - a)\left(\frac{P}{m(a/W)} \right)^{n_1} = (W - (a + \Delta a))\left(\frac{P - \Delta P}{m((a + \Delta a)/W)} \right)^{n_1}. \quad (6)$$

These calculations were applied to the HAZ A6I test corresponding to unaged material strained by 15%. Fig. 15 shows that a large load jump from 5.80 to 5.05 kN was observed only after 15 h. The application of Eq. (6) showed that the calculated propagation length was 1.25 mm which is consistent with the final experimental propagation length of 1.63 mm. This load decrease strongly suggests that crack initiation occurred at the very beginning of the test. This is the reason why a second relaxation test was performed on the very crack sensitive A6I HAZ material. This second test was interrupted after only 30 h. As reported in Table 4, the experimental intergranular crack propagation length is 1.1 mm which is of the same order of magnitude than that of the test which lasted 1000 h. Therefore, this last test clearly shows that crack propagation under stress relaxation occurs very early and explains the abrupt load jump observed on the global response. Furthermore, a third relaxation test on the same simulated HAZ was performed and stopped after the loading phase to check that there was no intergranular initiation during the loading phase. Here it should be added that a damage model based on local approach methodology identified [11] for these simulated HAZ and applied [12] to these relaxation tests predicted also that crack initiation, when it occurs, appears at the beginning of the test.

These interrupted tests raise an essential question about the effect of aging and Ti(C,N) precipitation on the stress relief cracking mechanism. X-rays examinations have shown that at 600 °C, 321 stainless steel predeformed by 20% leads to the precipitation of titanium carbides only after a hold time of about 20 h [22]. This indicates that significant intergranular crack propagation can occur without any significant Ti(C,N) precipitation, that is in a material containing a high amount of dislocations and solute atoms (Ti, C and N).

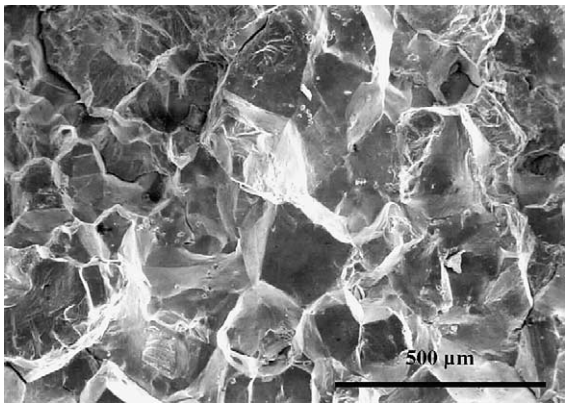

Fig. 17. Fracture surface of CT specimen after relaxation tests for an unaged and strained (15%) AISI 304H simulated HAZ.

To further investigate the role of Ti(C,N) particles, the same methodology of HAZ simulation was applied to a AISI 304H stainless steel in which such particles cannot be formed. The chemical composition of the material is given in Table 5. This composition is very similar to that of AISI 321 steel except the titanium content. In the as-received condition, the material has a grain size of 150 μm this is why the annealing treatment was applied at 1050 °C during 30 min to avoid any further grain growth. This treatment was followed by a cold rolling of 15% to produce simulated HAZs. A constant opening rate and a relaxation test on CT specimen were also performed (see Table 4). The relaxation test was interrupted after 30 h and the obtained crack propagation length was 1.8 mm. The fracture surface was also fully intergranular as observed in Fig. 17. This test clearly shows that work hardening plays a key role in intergranular cracking phenomenon. It shows also that the presence of Ti(C,N) particles is not a prerequisite for this form of damage observed under stress relaxation.

4. Discussion

Before discussing the mechanism(s) responsible for intergranular fracture observed under stress relief cracking conditions, we will first evaluate the effect of Ti

Table 5
Chemical analysis of the investigated AISI 304H sheet (wt%)

C	Mn	Si	Cr	Ni	Mo	S	P	Cu	Ti	Nb	B	N
0.059	1.23	0.68	18.4	11.8	0.33	0.03	0.028	0.12	<0.02	<0.05	0.0005	0.034

carbide precipitation on the mechanical properties since, in the literature, this precipitation is usually considered as responsible for this failure mode. The contribution of solid solution strengthening modified by Ti carbide precipitation and that of dislocation recovery on the hardness and the creep resistance of pre-deformed materials are also discussed. In order to define the role of titanium carbides on the mechanical properties, let us estimate the Orowan stress for each simulated HAZ, using the results of TEM observations. If ϕ is the particle diameter, f their volume fraction and λ the mean distance between particles, the Orowan stress at 600 °C, σ_{Orowan} can be expressed as:

$$\sigma_{\text{Orowan}} = M\frac{\mu \cdot b}{\lambda - \phi} \tag{7}$$

with

$$\lambda = \frac{\phi}{\sqrt{f}}. \tag{8}$$

The results are presented in Table 6 using $M = 3$, $\mu =$ 57 GPa and $b = 0.258$ nm. The calculated Orowan stress range is 200–300 MPa, which shows that precipitation of titanium carbides during aging at 650 °C can induce significant hardening. However, it should be kept in mind that hardening during aging was only observed in materials deformed by less than 15%. This indicates that other mechanisms than precipitation hardening are needed to explain the mechanical properties of the investigated materials. An attempt is made to detail them hereafter.

During aging titanium carbide precipitation could also be responsible for a loss of hardening by decreasing the amount of solute atoms like C, N and Ti. An analytical expression (Eq. (9)) for the variation of the yield stress as a function of chemical composition has been proposed [23] as:

$$\begin{aligned} Rp_{0.2}\ (\text{MPa}) = 15.4 \cdot [&4.4 + 23(\text{C}) + 32(\text{N}) \\ &+ 1.7(\text{Ti}) + 1.3(\text{Si}) + 0.24(\text{Cr}) \\ &+ 0.94(\text{Mo}) + 1.2(\text{V}) + 0.29(\text{W}) \\ &+ 2.6(\text{Nb}) + 0.82(\text{Al}) \\ &+ 0.16(\text{ferrite } \delta) + 0.46d^{-1/2}]. \end{aligned} \tag{9}$$

This expression shows that if all the carbon, nitrogen and titanium atoms precipitate, this leads to a decrease of 40 MPa for the yield stress. This decrease is smaller than that observed in the heavily cold rolled materials. This means that holding these HAZ materials at high temperature leads to a dislocation network rearrangement that can be responsible for a significant softening effect by recovery processes. Actually, the mechanical strength of these aged HAZ materials results from two opposite effects: (i) precipitation hardening by Ti(C,N) formation, and (ii) a softening effect due to solute atom disappearance and dislocation recovery.

Concerning the creep behaviour, aging is systematically associated with an increase of the creep rate. The secondary creep rate of these HAZ strongly depends on the stress level (the Norton exponent is equal to 22 for the 15% cold rolled and aged HAZ A.4.III). This value is anomalously high, since usually, this coefficient is of the order of 4 in solid solution materials [24]. These large values of the Norton exponents suggest that an internal stress has to be taken into account because the microstructure is necessarily restored under an effective stress smaller than the applied one. If for instance a Norton exponent is set equal to 4 for the 15% cold rolled and aged HAZ (A.4.III) material the stress dependence can be written as follows:

$$\overline{\mathrm{d}\varepsilon} = 6 \times 10^{-12}(\sigma - 289)^4 \tag{10}$$

with the time in hour and the stress in MPa. This would suggest the existence of an internal stress of the order of

Table 6
Secondary Ti(C,N) precipitation characteristics for different simulated HAZ

State reference	Cold rolling ratio (%)	Temperature (°C)	Duration (h)	ϕ (nm)	f (%)	λ (nm)	σ_{Orowan} (MPa)	$Rp_{0.2}$ (MPa)
A.6.I	15	–	–	–	–	–	–	475
A.3.III	15	650	500	3.8	0.036	200	225	434
A.4.III	15	650	1000	4.2	0.075	153	295	425
A.5.III	15	650	3000	4.7	0.105	145	315	424
A.7.III	15	650	10 000	5.5	0.135	150	305	–
A.7.II	15	600	10 000	3.9	0.035	208	215	436
C.6.I	5	–	–	–	–	–	–	246
C.5.III	5	650	3000	8.6	0.277	163	285	300
In-service aged base metal	0	550	90 000	16.9	0.556	227	210	205
In-service cracked HAZ	?	550	90 000	16	0.468	234	202	–

300 MPa. This value is close to the Orowan stress estimated for this HAZ material. However, this result cannot be applied to all aging conditions. We have seen that the more severe the aging, the higher the creep rate in spite of a more important Ti(C,N) precipitation and a higher corresponding value for the Orowan stress. Therefore, it can be concluded that secondary titanium carbides do not control alone the creep behaviour of these simulated 321 HAZs. Furthermore, we have also shown that the contribution of grain boundary sliding to overall creep strain is small. Therefore, it seems that neither titanium carbides nor grain boundary sliding can control the creep behaviour of these materials.

In this discussion on creep behaviour, another effect must be taken into account. Aging causes titanium carbide precipitation and therefore decreases the amount of solute atoms present in the austenitic matrix. This can facilitate the dislocation rearrangement and increase the recovery rate. It is therefore suggested that the creep behaviour is controlled by a solute drag effect, rather than by carbide precipitation or grain boundary sliding.

As stated in Section 1, the stress relief cracking of 321 HAZs is usually attributed to an hardening effect produced by Ti(C,N) precipitation during service at high temperatures [4–7]. It is assumed that intergranular cracking occurs in service when the ductility of the grains is no longer sufficient to sustain the relaxation of welding and clamping stresses. The results obtained in the present study are not fully consistent with this explanation which is widely used in the literature. Fig. 14 shows that work hardening is effectively the dominating parameter in the stress relief cracking mechanism. But it should also be noted that, if pre-straining is a pre-requisite for intergranular cracking during stress relaxation, static aging before loading is not. The mechanism of stress relief cracking has also been reproduced on cold rolled but unaged materials. Moreover, it was shown that intergranular crack propagation occurs in the very first hours (<30 h) in the absence of any significant carbide precipitation. Intergranular cracking during stress relaxation was also observed in AISI 304H simulated HAZ. This raises serious doubts about the role of Ti(C,N) precipitation on stress relief cracking mechanism.

It is suggested that another mechanism is operative from the very beginning of the stress relaxation test in the absence of any carbide precipitation. It is believed that solute drag effect might be this mechanism. It is well to remember that the presence of C, N and Ti atoms in solid solution is important to explain the tensile properties. It has been shown above that these atoms play a significant role on creep properties. This is why we suggest that, without any aging, these solute atoms may impede the motion of the numerous dislocations introduced by cold rolling and therefore can be responsible for the modification of the recovery mechanisms. The interaction between solute atoms and dislocations reduces the recovery rate and maintains large values for the local internal stresses responsible for the nucleation of creep cavities along the grain boundaries. This mechanism proposed for stress relief cracking is different from the explanation which is usually given in the literature devoted to this phenomenon [1–7].

5. Conclusions

HAZs of AISI 321 stainless steel have been simulated using an annealing heat treatment at 1200 °C for 15 min, followed by cold rolling (<40%) and thermal aging at 550, 600 and 650 °C. Three main conclusions can be drawn from microstructural observations combined with tensile, creep, and stress relaxation tests on pre-cracked specimens performed at 600 °C.

1. The hardness and the tensile strength are increased by thermal aging at 650 °C for low amounts of cold rolling (<15%). These properties are decreased by thermal aging at 650 °C for larger amounts of cold rolling. Creep time to failure is decreased while creep strain rate is increased by thermal aging in all cases. These variations in mechanical properties result from a competition between secondary Ti(C,N) precipitation (Orowan mechanism), a decrease of solute drag effect (especially in creep tests) and a decrease of the work hardening contribution due to the recovery of dislocation microstructure introduced by cold pre-straining.
2. Ti carbide precipitation is not the pre-dominant mechanism responsible for intergranular cracking observed in slow strain rate tests and stress relaxation tests performed on pre-cracked specimens at 600 °C. A mechanism based on the existence of large local internal stresses introduced by cold pre-straining is proposed. These internal stresses are assumed to be responsible for the accelerated nucleation rate of intergranular creep cavities. These local internal stresses are not easily relaxed because of the interactions between dislocations and solute atoms in solid solution, while transgranular strengthening effect due to carbide–dislocation interactions seems to play a minor role. Pre-straining which is the source of these internal stresses remains a pre-requisite for the formation of intergranular cracks during stress relaxation.
3. The number and the size of titanium carbide precipitates are an excellent indication of the amount of pre-straining which is the dominant factor for intergranular fracture. Moreover, the stage reached by this precipitation directly reflects the presence of solute atoms (C, N, Ti) left in solid solution for a given thermo-mechanical condition.

References

[1] R.M. Curran, A.W. Rankin, Trans. ASME (1957) 1398.
[2] R.D. Thomas, Weld. Res. J. (1984) 24.
[3] R.D. Thomas, Suppl. Weld. Res. J. (1984) 355.
[4] C.F. Meitzner, Weld. Res. Council Bull. 211 (1975) 1.
[5] J.C. Van Wortel, Maintenance for managing life performance, 1998, p. 637.
[6] A. Dhooge, Weld. World 41 (1998) 206.
[7] C. Picker, Nucl. Energy 3 (1992) 207.
[8] R.N. Younger, D.M. Haddrill, R.G. Backer, J. Iron Steel Inst. (1963) 693.
[9] A. Dhooge, A. Vinckier, Int. J. Pres. Ves. Piping 27 (1987) 239.
[10] M. Chabaud-Reytier, PhD thesis, Ecole Nationale Supérieure des Mines de Paris, 1999.
[11] M. Chabaud-Reytier, L. Allais, D. Poquillon, C. Caes-Hogrel, M. Mottot, A. Pineau, Mater. High Temp. 18 (2) (2001) 71.
[12] D. Poquillon, M. Chabaud-Reytier, L. Allais, A. Pineau, Mater. High Temp. 18 (2) (2001) 82.
[13] M. Chabaud, L. Allais, I. Chu, P. Dubuisson, A. Pineau, in: Proceedings of ECF 12'Fracture from Defects', Sheffield, England, 14–18 September 1998, Engineering Materials Advisory Services, 1998, p. 429.
[14] L. Allais, M. Bornert, T. Bretheau, D. Caldemaison, Acta Metall. Mater. 42 (11) (1994) 3865.
[15] F. Lecroisey, A. Pineau, Metall. Trans. 3 (1972) 387.
[16] J.D Cook, D.R. Harries, A.C. Roberts, in: Proceedings Conference on Creep Strength in Steel and High Temperature Alloy, Sheffield, UK, 20–22 September 1972, The Metals Society, London, 1974.
[17] F.E Asbury, G. Willoughby, in: Proceedings Conference on Creep Strength in Steel and High Temperature Alloy, Sheffield, UK, 20–22 September 1972, The Metals Society, London, 1974.
[18] J.M. Adamson, J.W. Martin, in: Proceedings Conference on Creep Strength in Steel and High Temperature Alloy, Sheffield, UK, 20–22 September, The Metals Society, London, 1974.
[19] R.J. Truman, H.W. Kirkby, Journal of Iron and Steel Institute (1960) 180.
[20] Q. Auzoux, L. Allais, A.F. Gourgues, A. Pineau, in: Proceedings of 14th Biennal European Conference on Fracture, Cracovie, Poland, 8–13 September 2002, EMAS Publications, Sheffield, 2002.
[21] P. Bensussan, R. Piques, A. Pineau, in: A. Saxena, J.D. Landes, J.L. Bassani (Eds.), Nonlinear Mechanics: Volume I, Time Dependent Fracture, ASTM, Philadelphia, 1989, p. 27.
[22] A.S. Grot, J.E. Spruiell, Metall. Trans. 6A (1975) 2023.
[23] F.B. Pickering, Physical Metallurgy and Design of Steels, Applied Science, London, 1978.
[24] H.F. Frost, M. Ashby, Deformation Mechanisms Maps, Pergamon, Oxford, 1982.